EVALUATION OF CONSUMER-GRADE AND SURVEY-GRADE UAV-LIDAR

G. Mandlburger[1],[*] M. Kölle[2], F. Pöppl[1], M. Cramer[2]

[1] TU Vienna, Department of Geodesy and Geoinformation, Vienna - (gottfried.mandlburger, florian.poeppl)@geo.tuwien.ac.at
[2] University of Stuttgart, Institute of Photogrammetry - (michael.koelle, michael.cramer)@ifp.uni-stuttgart.de

KEY WORDS: Unmanned Aerial Vehicles, Laser Scanning, Low-Cost Sensor, Accuracy Assessment

ABSTRACT:

Driven by developments in the automotive industry, the availability of compact consumer-grade LiDAR (Light Detection and Ranging) sensors has increased significantly in recent years. Some of these sensors are also suitable for UAV-based surveying tasks. This paper first discusses the differences between consumer-grade and survey-grade LiDAR systems. Special attention will be paid to the scanning mechanisms used on the one hand and to different solutions for the transceiver units on the other hand. Based on the technical data of two concrete systems, the consumer-grade *DJI* Zenmuse L1 sensor and the survey-grade scanner *RIEGL* VUX-1UAV, the expected effects of the sensor parameters on the 3D point cloud are first discussed theoretically and then verified using an exemplary data set in Hessigheim (Baden-Württemberg, Germany). The analysis shows the possibilities and limitations of consumer-grade LiDAR. Compared to the low-cost sensor, the high-end scanner exhibits lower range measurement noise (5-10 mm) and better 3D point location accuracy. Furthermore, the higher laser beam quality of high-end devices (beam divergence, beam shape) enables more detailed object detection at the same point density. With moderate accuracy requirements of 5-10 cm, however, applications in the geodetic-cartographic context also arise for the considerably less expensive consumer-grade LiDAR systems.

1. INTRODUCTION

In the past 20 years, Unmanned Aerial Vehicles (UAV) or drones, respectively, have been increasingly used for 3D data acquisition. Due to their low weight, compact and mirror-less camera systems were initially used for this purpose (Colomina and Molina, 2014). Thanks to advancing miniaturization, it is now also possible to integrate compact laser scanners on UAVs (Nex et al., 2022). Powerful platforms even allow the installation of hybrid sensor systems consisting of cameras and laser scanners (Mandlburger, 2022).

In the development of lightweight scanner systems, the following two approaches can be distinguished: (i) scanners that have emerged from established Airborne Laser Scanning (ALS) systems as an evolution of scanners explicitly designed for survey-grade data acquisition and 3D mapping, and (ii) scanners developed for detection of local surroundings and obstacles as a component of driver assistance systems in the automotive industry. In the first group, the main focus is on precision, accuracy and point density. Due to these requirements, the systems available on the market are usually expensive with acquisition costs in the range of 100K Euro. Devices of this type are too expensive for mass production, which is why low-cost sensors come primarily from the second sector.

In recent years, low-cost scanners representing a mixture between established conventional and so called profile array scanners have been introduced in the market (Liu et al., 2022). While the conventional systems feature (i) a single pulsed laser diode (PLD) as emitter, (ii) a single Avalanche Photo Diode (APD) as detector and (iii) beam deflection via a rotating or oscillating mirror, profile array scanners, also referred to as multi-beam LiDAR (Light Detection And Ranging), do not require a beam deflection unit but use a fan of 16-128 LiDAR transceivers rotating around a common axis (Altuntas, 2023, Schwarz,

2010). For obtaining high point density with a conventional system, the laser must provide high pulse repetition rate, and, together with precise detectors, such sensors are expensive. On the other hand, profile array scanners require accurate alignment of each PLD with the corresponding APD, which is not trivial and thus, again, hampers mass production.

The low-cost scanner system introduced in (Liu et al., 2022) uses a hybrid approach with six laser beams from pulsed laser diodes, which are deflected by a so-called Risley prism (Schwarze et al., 2013). The backscattered signal components are detected by associated APD receivers. This allows compact design and comparatively cheap production with costs in the range of 1K Euro for the LiDAR unit. This scanning system has grown in popularity and prevalence since about mid-2021 due to its use in the Zenmuse L1 product from the well-known drone manufacturer *DJI* (Kersten et al., 2022). In addition to the LiDAR unit, the Zenmuse L1 system is also equipped with a 20 Mpix fish-eye camera and a navigation system. This constitutes a complete ALS system at a price of approximately 10K Euro.

The lower price naturally entails sacrifices in terms of precision and accuracy. In this paper, therefore, first the sensor technology of the low-cost, consumer-grade system is examined and the effects of the components used on the quality of the 3D point cloud are discussed (Section 2). For the practical comparison, a concrete data set in Hessigheim (Baden-Württemberg, Germany) is available, which was flown in March 2021 with the high-quality scanner system *RIEGL* VUX-1UAV and in March 2022 with the low-cost sensor *DJI* Zenmuse L1. The data set and data analysis methods are described in Section 3. The obtained results are presented and critically discussed in Section 4. The paper ends with a summary of the main findings in Section 5.

---

[*] Corresponding author

The International Archives of the Photogrammetry, Remote Sensing and Spatial Information Sciences, Volume XLVIII-1/W3-2023
2nd GEOBENCH Workshop on Evaluation and BENCHmarking of Sensors, Systems and GEOspatial Data
in Photogrammetry and Remote Sensing, 23–24 October 2023, Krakow, Poland

2. SENSOR TECHNOLOGY

In this section, the basic components of a UAV laser scanning system are first introduced (Section 2.1). The central elements of a scanner, namely the laser range finder and the beam deflection unit, are then described for both high-end and low-cost sensors in Sections 2.2 and 2.3. Finally, Section 2.4 compares the parameters of the VUX-1UAV survey-grade sensor and the Livox Avia consumer-grade laser scanner installed in the Zenmuse L1 and discusses the expected impact on the quality of the 3D point cloud.

2.1 System components

UAV laser scanning is not fundamentally different from conventional ALS operated from piloted platforms in terms of the components used. In both cases, it is a multi-sensor system consisting of a satellite navigation receiver (GNSS, Global Navigation Satellite System) and an inertial measurement unit (IMU) for recording the position and orientation of the measurement platform, and the laser scanner consisting of the ranging (LiDAR) and the beam deflection (scanning) unit. The 3D point coordinates on the ground are calculated from the measurement data of the multi-sensor system using direct georeferencing (Vosselman and Maas, 2010, Shan and Toth, 2018, Pöppl et al., 2023). This takes into account the scanner measurements (distance, deflection angle) and the position and orientation computed by the GNSS/IMU navigation unit.

Here, an error in the coordinates of the measurement platform has a direct effect as a 3D point location error of the object points. This means that even for UAV-based laser scanning, high demands are placed on the GNSS receivers. The situation is different for orientations. Due to the much shorter measuring distance of approx. 50-120 m, IMUs with lower accuracy can be used for UAV laser scanning than is the case for ALS from piloted platforms with measuring distances of 500-4000 m. The same applies analogously to the range finder and the scanning unit of the laser scanner, where errors in distance measurement have a direct effect on the height component of the measurement points for beam directions in the nadir direction, and errors in the deflection angles have a less serious effect due to the short lever arm (Mandlburger, 2022). As in ALS, however, strict time synchronization of all components involved in the kinematic measurement system is also required in the UAV case.

2.2 LiDAR unit

In ALS, laser ranging is based on the Time-of-Flight (ToF) principle. This applies to operation from both crewed and uncrewed platforms. A short laser pulse of about 3-5 ns duration (equivalent to 90-150 cm length in metric units) is emitted and the time between emission and arrival of the reflected received signal is measured. There are differences in the details of echo detection, with the most precise determination being made by recording the full echo waveform (Full Waveform, FWF) of the backscattered laser signal (Mallet and Bretar, 2009). In this process, the strength of the received signal is sampled and digitized at a frequency of 1-2 GHz, and from this the signal travel time to a specific object is determined either online or in post-processing (Pfennigbauer et al., 2014). The prior is referred to as Online Waveform Processing (OWP) and delivers additional attributes characterizing each laser echo like amplitude, reflectance and pulse shape deviation, a measure describing the quality of the echo pulse.

Furthermore, FWF laser scanning also allows the derivation of additional attributes such as signal amplitude and pulse broadening (Jutzi and Stilla, 2006, Wagner et al., 2006). FWF technology is also available for high-end UAV laser scanners. A simpler but less precise detection method is to measure the transit time via a component known as a Time-to-Analog Converter (TAC). Once the reflected echo signal exceeds a certain strength, this triggers a stop pulse. Such a solution is called a discrete echo system and is typically used in low-cost devices.

2.3 Scanning concepts

UAV laser scanners partly use conventional concepts of beam deflection via oscillating, rotating or nutating mirrors or polygon wheels. Some common implementations are listed in Figure 1, which shows the scanning mechanism at the top and the resulting point pattern on the ground at the bottom. Compared to ALS sensors from crewed platforms, which have a total scanner Field-of-View (FoV) of typically $\pm 30°$ around the nadir direction, scanning mechanisms that allow $360°$ beam deflection are also used in the UAV case (Figure 1b). This is particularly advantageous when scanning narrow street canyons, river corridors and mountain valleys. This scanning concept usually uses a single LiDAR unit consisting of a high-quality laser source and receiving diode. Devices of this type are mainly used in high-end equipment for precise measurement tasks (Mandlburger, 2022).

For consumer-grade sensors, two scanning concepts are predominant: (a) Rotating multi-beam laser scanners do not use beam deflection but multiple LiDAR transceiver units (typically 16, 32, 64, 128). Pulsed diode lasers are usually used for each source and there is a corresponding photo-diode for each laser source (Alsadik, 2020, Altuntas, 2023). The entire transceiver bundle rotates around a common axis. The concept was primarily developed for use in the automotive industry and also allows $360°$ scans. (b) Also from the automotive industry comes a hybrid concept that uses a small number of static LiDAR units, typically consisting of six PLD/APD transceivers (Liu et al., 2022). The laser beams are deflected by refraction over a so-called Risley prism (Figure 2). Risley prisms consist of two bevelled glass wedges that can be operated (i) either in the same direction or in opposite directions, and (ii) with the same or different rotation speed. By adapting the two parameters, different scanning patterns result on the ground, ranging from simple scan lines to scan circles and figure-of-eight loops (cf. Figure 2b+c), to spirals and complex petal patterns. For aerial mapping tasks, the advantage is that this scan concept can be used to look forward, backward and sideways. The disadvantage is that the refractive deflection concept causes a degradation of the beam quality due to scattering effects in the glass.

2.4 Comparison of sensor specifications

Table 1 shows that the survey-grade system exhibits a ranging accuracy that is better by a factor of four compared to the consumer-grade system and an angular accuracy of the IMU that is better by a factor of two. Neglecting GNSS errors, this results in a point position accuracy of about 1 cm for the survey-grade and 5 cm for the consumer-grade system.

There is also a difference with respect to the laser beam quality. While the laser beam cone of the high-end VUX-1UAV is circular with a beam divergence of 0.5 mrad, corresponding to a circular laser footprint diameter of 25 mm (in nadir direction) at a flight altitude of 50 m above ground level (agl), the laser

The International Archives of the Photogrammetry, Remote Sensing and Spatial Information Sciences, Volume XLVIII-1/W3-2023
2nd GEOBENCH Workshop on Evaluation and BENCHmarking of Sensors, Systems and GEOspatial Data
in Photogrammetry and Remote Sensing, 23–24 October 2023, Krakow, Poland
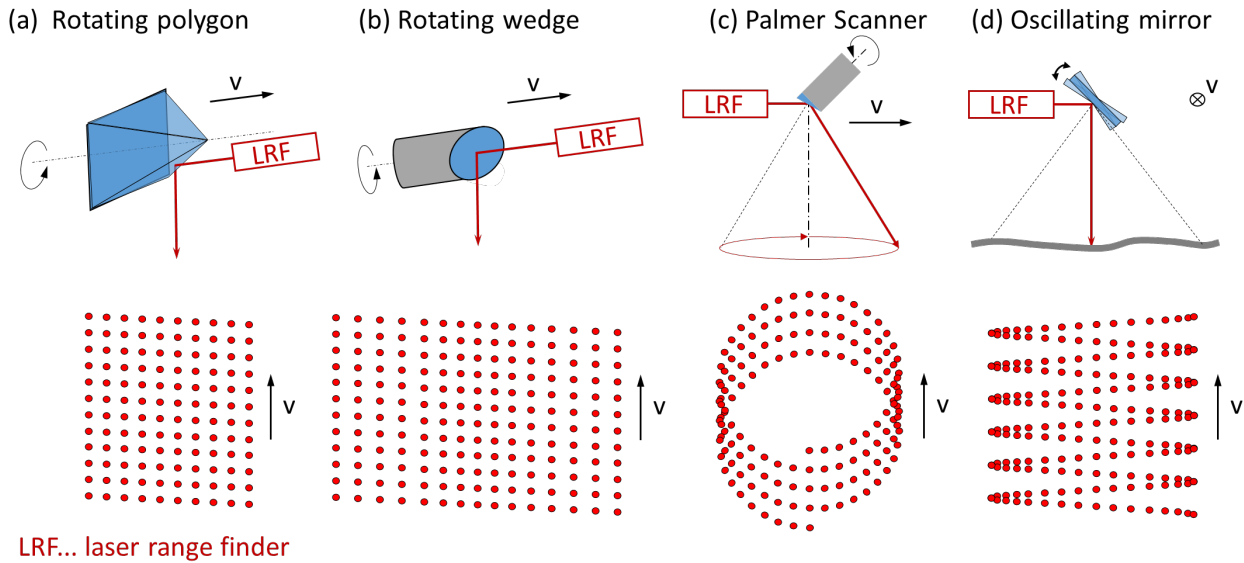
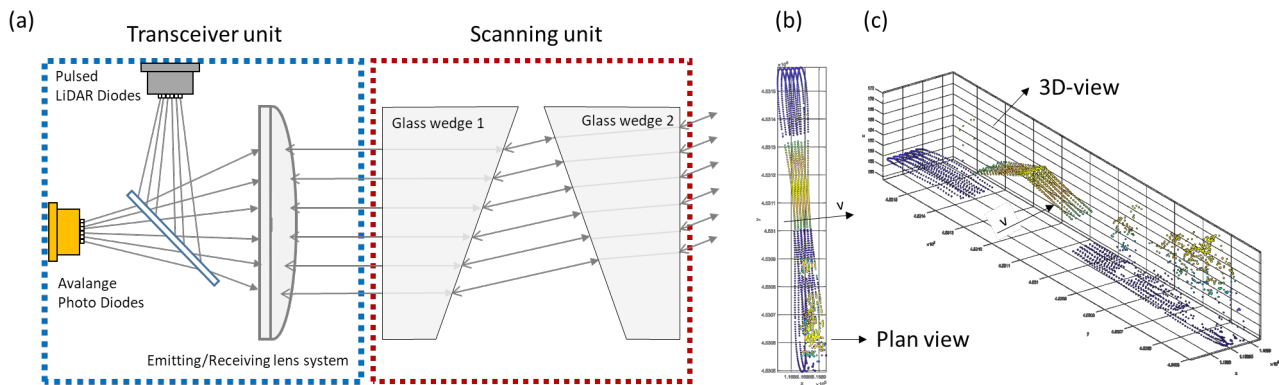Figure 1. Scanning mechanisms and scan patterns in conventional laser scanning.

Figure 2. (a) LiDAR and scanning unit of the Livox Avia (principle sketch after Liu et al., 2021); (b+c) plan view and 3D-perspective view of laser points during a full rotation of the scanning unit (six parallel figure-of-eight-shaped scan curves).

beam of the consumer-grade Zenmuse L1 has a pronounced elliptical shape with a major semi-axis of 250 mm at a flying altitude of 50 m agl. The size of the scanning spot, together with the point spacing, determines the spatial resolution of a scanner system. Therefore, for the survey-grade system, a spatial resolution in the range of a few centimeters can be expected. For the consumer-grade sensor, the spatial resolution is several decimeters even with a small point spacing and is therefore an order of magnitude worse than for the high-end system.

	VUX-1UAV	Zenmuse L1
Wavelength [nm]	1550	905
Max range ρ=20% [m]	750	230
Nr. of transceivers	1	6
Scan rate [kHz]	1200	240
Field of view [○]	360	70
Footprint $\varnothing$@h=50m [mm]	25	35x250
Ranging accuracy [mm]	5	20
Acc. scan angle [°]	0.001	0.050
Acc. roll+pitch [°]	0.015	0.025
Acc. heading [°]	0.035	0.080
Echo detection	OWP	up to 3
RGB Camera [MPix]	2 x 24	1 x 20
Weight [kg]	3.75	0.93

Table 1. Sensor specifications

3. DATA SETS AND EVALUATION METHODS

For a practical comparison of the consumer-grade Zenmuse L1 UAV laser scanning system discussed in the previous section with the survey-grade VUX-1UAV sensor, aerial surveys were conducted in Hessigheim (Baden-Württemberg, Germany, Figure 3). This area has been the subject of research on high-precision UAV surveying using stereo photogrammetry and laser scanning for several years (Cramer et al., 2018, Haala et al., 2022). 3D point clouds of this data set acquired with the high-end system are publicly available as part of the ISPRS H3D benchmark (Kölle et al., 2021). The acquisition with the *RIEGL* VUX-1UAV took place in March 2021. One year later, in March 2022, the same area was acquired with the *DJI* Zenmuse L1 sensor.

Figure 3 shows an orthophoto of the study area as image background and a DEM shading derived from the respective 3D laser point cloud as foreground. For the VUX data set the positions of the two oblique cameras are additionally plotted for the western part of the study area to visualize the flight trajectory (Figure 3a). For the L1 data set (Figure 3b), the entire flight path is drawn. Here, data acquisition was divided into three individual flights: blue/red: eastern/ western block with north-south flight strips and green: southern block with east-west cross strips.

The International Archives of the Photogrammetry, Remote Sensing and Spatial Information Sciences, Volume XLVIII-1/W3-2023
2nd GEOBENCH Workshop on Evaluation and BENCHmarking of Sensors, Systems and GEOspatial Data
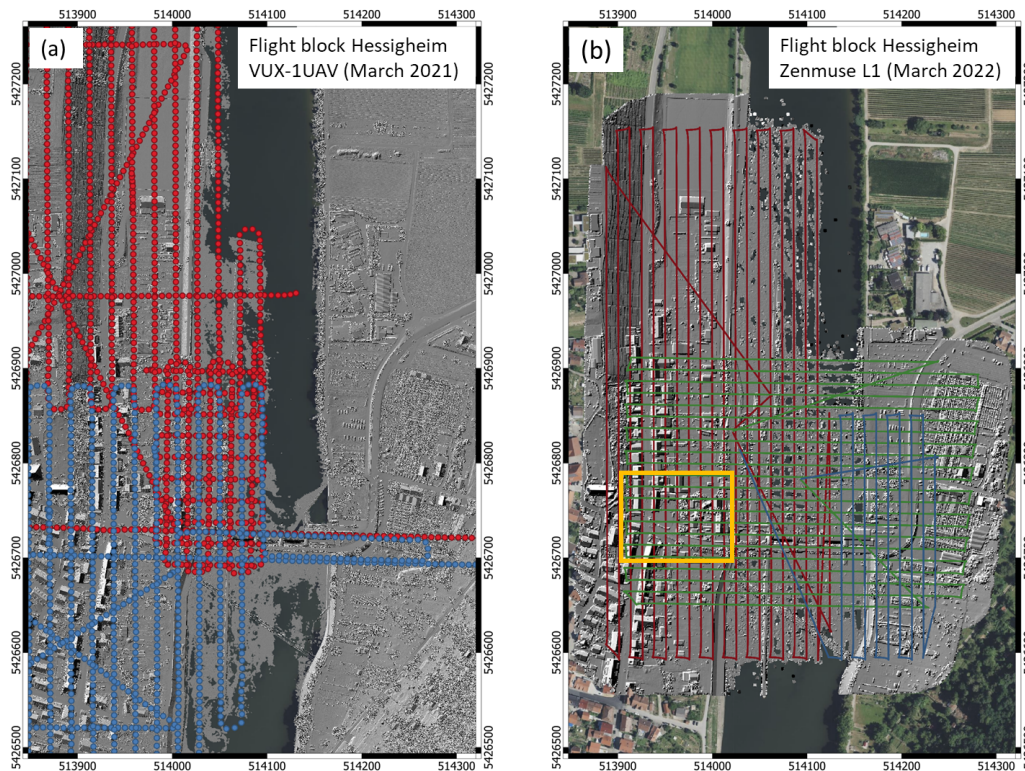in Photogrammetry and Remote Sensing, 23–24 October 2023, Krakow, Poland

Figure 3. Study area Hessigheim; left: VUX-1UAV (March 2021), Orthophoto and DEM shading + camera positions of the two western flight blocks; right: Zenmuse L1 (March 2022), Orthophoto and DEM shading + trajectories of the three flight blocks, orange rectangle: detail area of Figures 4, 5, and 6.

For the precise georeferencing of the individual flights, saddle-roof-shaped control surfaces on the one hand and checkerboard control points on the other hand were used as reference (Cramer et al., 2018, Haala et al., 2022). The position of the reference points and surfaces was measured with sub-centimeter accuracy using GNSS and total stations (according to the adjustment protocols of the terrestrial survey), and the heights were determined using leveling. The fitting accuracy of the 3D point clouds of the individual flight strips was checked with the scientific laser scanning software OPALS (Pfeifer et al., 2014) before and after rigorous strip adjustment (Glira et al., 2019).

The employed strip adjustment procedure uses (i) the time-stamped flight trajectory (GPS time, x, y, z, roll, pitch, yaw) and (ii) the 3D laser points in the scanner's own Cartesian coordinate system as primary input. Initial data processing (Kalman filtering of GNSS/IMU data and 3D point cloud generation) was carried out with the *DJI* Terra software. The resulting 3D point cloud in WGS84/UTM coordinates was then further processed with the OPALS software to obtain local coordinates in the scanner system. The employed strip adjustment method enables estimation of boresight alignment (lever arm, boresight angles), sensor calibration parameters (range and scan angle offsets and scales), and trajectory optimization with constant (bias) and spline-based correction models (Glira et al., 2016). By analyzing the residual height discrepancies after strip adjustment, conclusions can be made about the respective quality of (i) the navigation unit and (ii) the scanner used. Beyond the quantitative evaluation, a visual analysis of the derived point clouds was also performed.

4. RESULTS AND DISCUSSIONS

Figure 4 shows the height deviations of overlapping flight strips for two L1 flight blocks. Green-blue shades indicate positive and yellow-red shades negative height deviations of 2-10 cm. If the height difference of the overlapping strips is less than 2 cm, the areas are shown in white. Figure 4 represents the situation after data processing in the *DJI* Terra software.

One can see clear transitions of the color tones from red to blue in the overlap area (blue outlined rectangles), i.e. of height differences that run from about -10 cm to +10 cm, suggesting an error in the determination of the roll component of the boresight angles. Furthermore, in the purple-bordered boxes in Figure 4, the height difference maps show a sudden change in color right at the ridge line for sloped roof surfaces, indicating systematic positional errors in the flight trajectory. This preliminary analysis indicated that improving the sensor orientation and georeferencing of the laser points using rigorous strip adjustment as described in the previous section is necessary. The results after strip adjustment are summarized in Figure 5 and contrasted with the VUX-1UAV reference data set.

Figure 5 shows the strip height differences of the VUX-1UAV data set (a) and the raw state (b) as well as different variants of the strip adjustment of the L1 flight block (c+d). For the absolute georeferencing of the L1 flight block within the strip adjustment procedure, selected roof areas of the VUX-1UAV data set were used. This data set serves as a reference due to its higher accuracy (Haala et al., 2022). The height deviations of overlapping flight strips here are <2 cm in 90 % of the cases and the robustly estimated standard deviation (σ_{MAD}) is 7 mm.

The International Archives of the Photogrammetry, Remote Sensing and Spatial Information Sciences, Volume XLVIII-1/W3-2023
2nd GEOBENCH Workshop on Evaluation and BENCHmarking of Sensors, Systems and GEOspatial Data
in Photogrammetry and Remote Sensing, 23–24 October 2023, Krakow, Poland
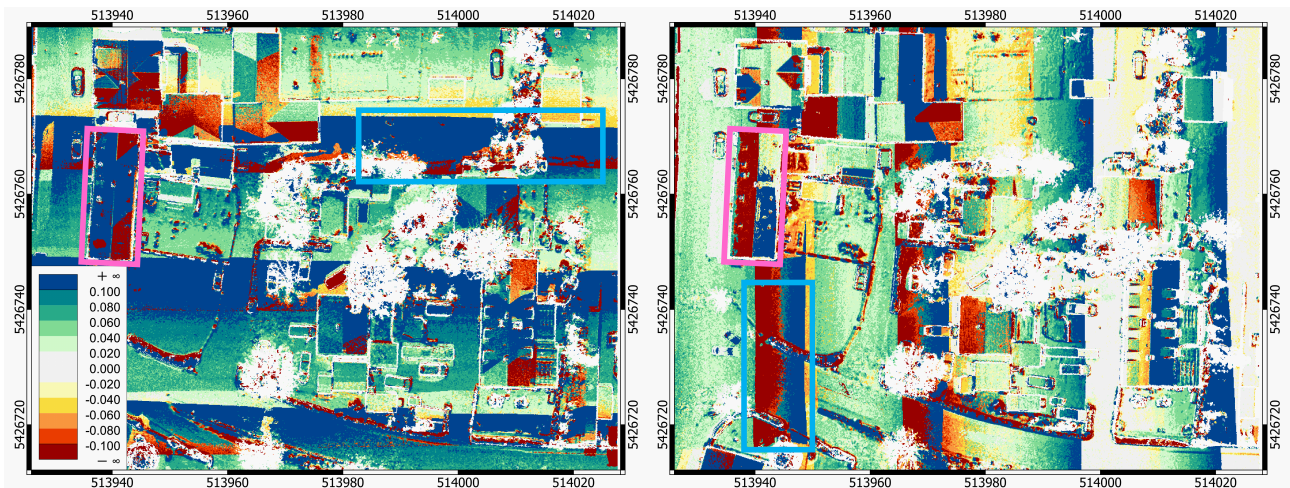

Figure 4. Strip height differences of two L1 flight blocks (green/red trajectories in Figure 3) after direct georeferencing using the Terra software.
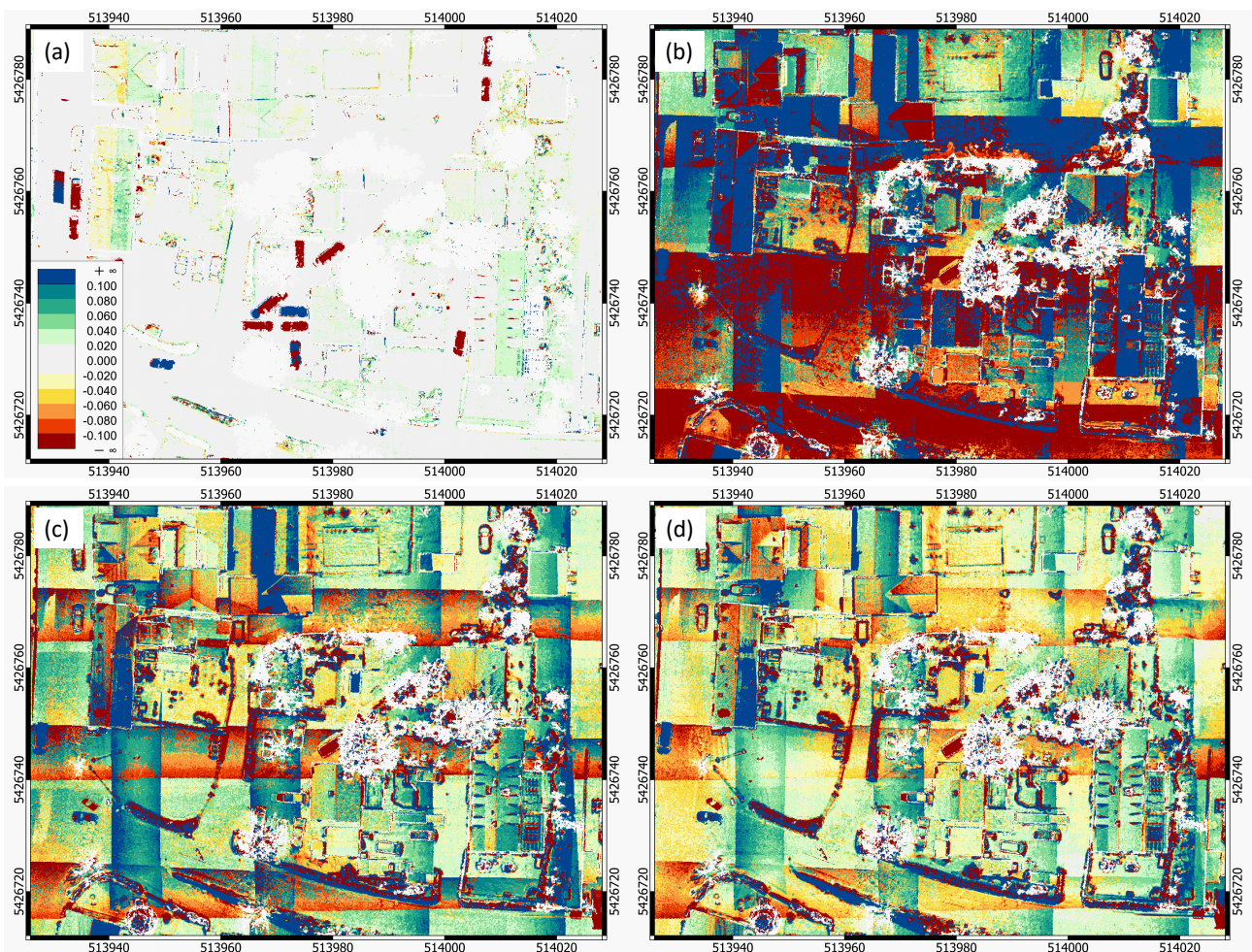

Figure 5. Strip height differences for the calibrated VUX-1UAV reference flight block (a), the raw state of Zenmuse L1 flight block (b), and after strip adjustment of the Zenmuse L1 block based on trajectory correction using bias model (c) and spline model (d).
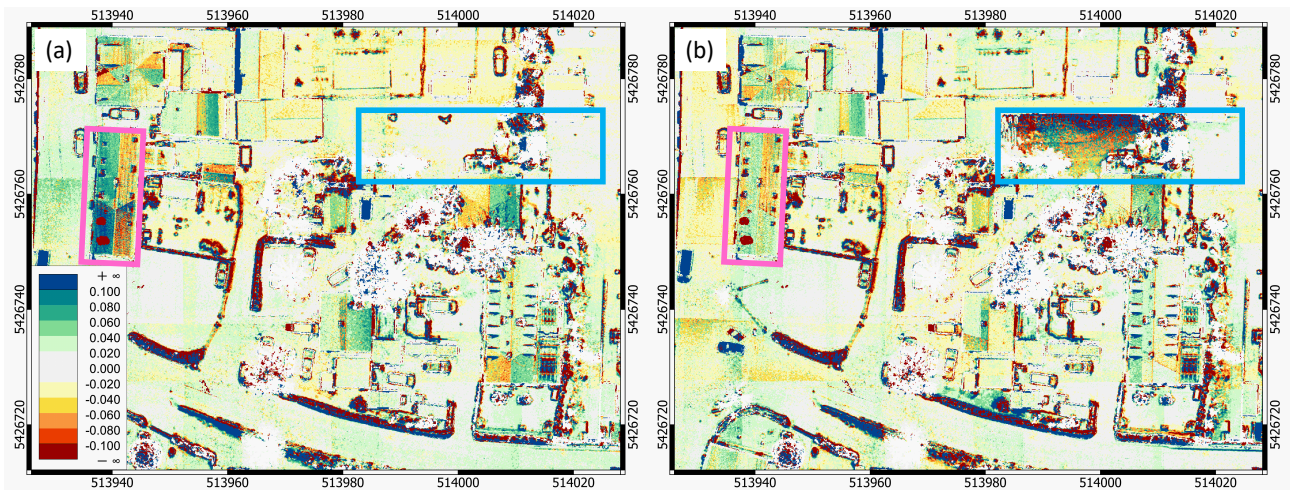
The International Archives of the Photogrammetry, Remote Sensing and Spatial Information Sciences, Volume XLVIII-1/W3-2023
2nd GEOBENCH Workshop on Evaluation and BENCHmarking of Sensors, Systems and GEOspatial Data
in Photogrammetry and Remote Sensing, 23–24 October 2023, Krakow, Poland

Figure 6. Strip height differences using points with a scan angle $\leq 25\,^\circ$; trajectory correction using bias model (a) and spline model (b).
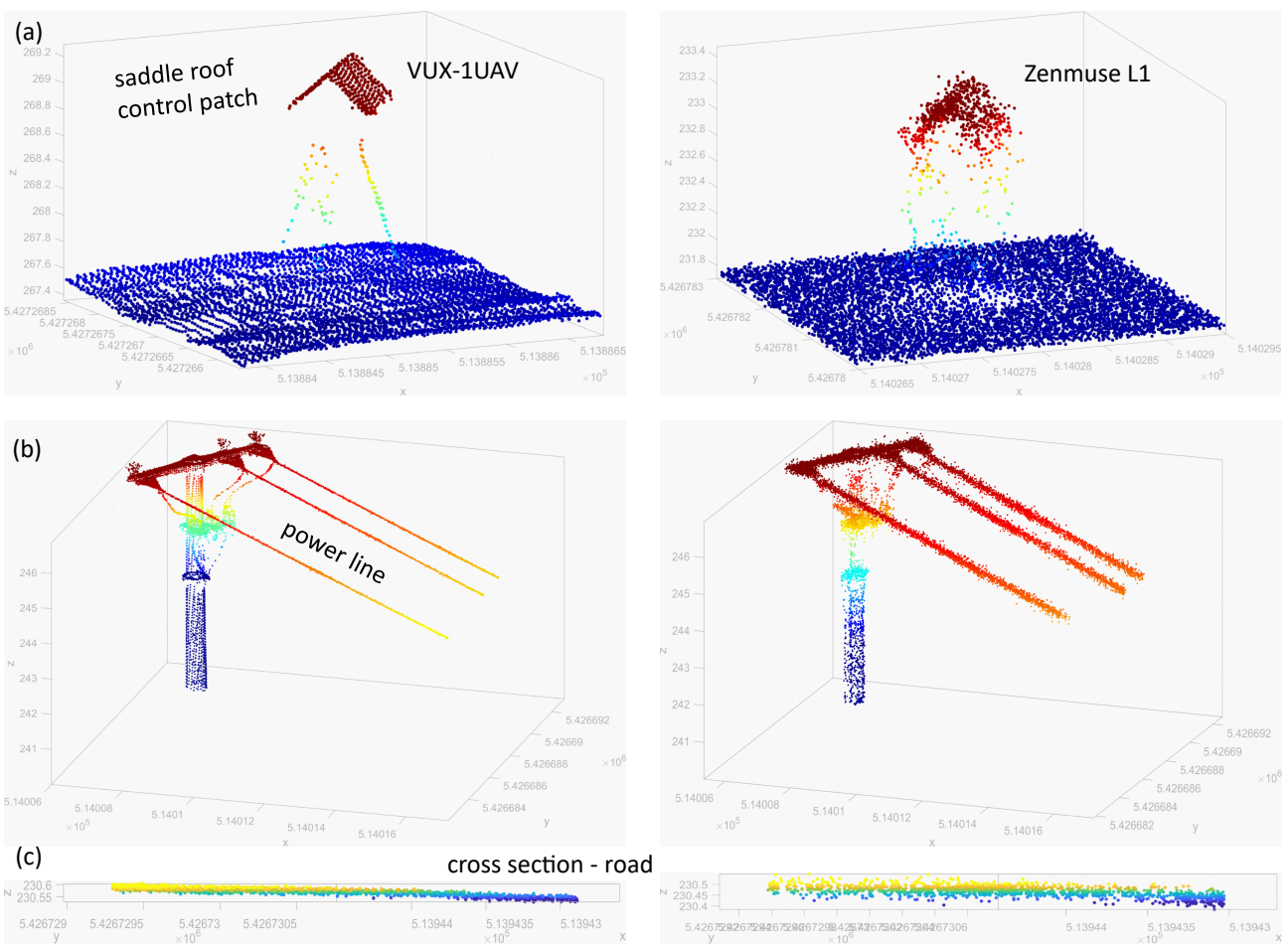

Figure 7. Point cloud comparison: VUX-1UAV (left) vs. Zenmuse L1 (right); (a) saddle roof-shaped control patch; (b) powerline pole and wires; (c) road cross section.

The International Archives of the Photogrammetry, Remote Sensing and Spatial Information Sciences, Volume XLVIII-1/W3-2023
2nd GEOBENCH Workshop on Evaluation and BENCHmarking of Sensors, Systems and GEOspatial Data
in Photogrammetry and Remote Sensing, 23–24 October 2023, Krakow, Poland

Figure 5a only shows larger height deviations at dynamic objects (vehicles). The VUX-1UAV reference is first contrasted with the height deviations derived from the raw L1 flight block (Figure 5b). In contrast to Figure 4, longitudinal and transverse stripes were examined together. While the height deviations shown in Figure 4 are mostly <10 cm, the flight blocks processed independently in the *DJI* Terra software show considerably larger height deviations among each other (σ_{MAD}=17 cm). This can be seen as a first indication that the GNSS/IMU navigation unit is one of the accuracy bottlenecks of the consumer-grade L1 system.

Starting from this state, Figure 5c+d show the state after strip adjustment, where the following parameters were determined: (i) the angular misalignment between the IMU and scanner systems (boresight misalignment), (ii) a range scale, and (iii) trajectory correction parameters. In the first case, a constant trajectory offset (bias) was estimated for each flight strip for each of the three positional and angular components (X, Y, Z, roll, pitch, heading). The results are shown in Figure 5c. Compared to the raw condition, the deviations with the bias correction model are considerably smaller (σ_{MAD}=8 cm), but the systematic effects cannot be completely compensated. This is recognizable by the saturated colors in the elevation difference map, especially at the strip boundaries. With such a simple correction model, it is not possible to achieve cm-accuracy.

A slightly further improved result is shown in Figure 5d. In this variant, a cubic spline curve was applied for each flight strip to correct the trajectory errors in all six components. Thus, also non-constant or non-linear error components can be compensated and σ_{MAD} decreases to 6.5 cm. However, it should be noted that even in this variant systematic deviations are still visible at the strip boundaries and at steep slopes. In general, the use of the spline correction is only recommended if sufficient reference data are available to support the entire flight block (Glira et al., 2019). The latter, however, contradicts the low-cost idea.

Starting from the observation that the highest deviations always occur at the strip boundaries, further analysis revealed a correlation of the height deviations with the scan angle. Although the applied strip adjustment model also allows to consider scan angle offsets and scales, the functional model was not able to sufficiently compensate the remaining systematic errors. Inspired by (Brazeal et al., 2021), who reported that additional calibration of the Risley prism-based scanning system is necessary for the used Livox sensors, and observing that high discrepancies predominantly occur for large positive scan angles, we restricted the laser data to points with scan angles less than +25° and repeated the strip adjustment with this set of input points. Due to the very high overlap of the scan data of more than 50 %, this was a feasible approach in this case.

The results are shown in Figure 6. From this figure, it can be seen that the fitting accuracy of the flight strips improved considerably for both variants of the trajectory correction. In the version with bias trajectory correction shown in Figure 6a, some remaining discrepancies are visible on the roofs (cf. purple box), while most of the systematic effects at the strip boundaries were successfully compensated (cf. blue box). The situation is reversed for the spline trajectory correction (Figure 6b), where the height discrepancies on the roof surfaces could be largely mitigated at the expense of occasional residual errors on the flat terrain. In both cases the overall height deviations are unbiased (mean: 0.0 cm and the robustly estimated standard deviation (σ_{MAD}) amounts to 3.8 cm. The fact that error metrics do not improve when using the more flexible spline trajectory correction model suggests that residual scanner calibration deficiencies are limiting the georeferencing accuracy rather than the GNSS/IMU navigation device. It is noted that, compared to the survey-grade system, the fitting accuracy is almost an order of magnitude worse for the consumer-grade sensor, but still below the decimeter.

In addition to the quantitative analysis, a visual comparison also shows the differences in data quality between the survey- and consumer-grade system. Figure 7 depicts the 3D point cloud for three selected areas of interest. The focus is on small and linear objects. As a representative example, Figure 7a shows one of the 40 x 80 cm^2 saddle roof-shaped control patches used for georeferencing the flight block and Figure 7b shows a power-line (pole and wires). In the data set of the consumer-grade system, the shape of the control patch is only dimly captured, which is due to moderate distance measurement accuracy on the one hand but mainly to the large (elliptical) laser footprint on the other hand. In the data set of the survey-grade sensor, the shape of the control patch can be recognized concisely in the point cloud with clearly pronounced flat areas. Only in the ridge area, footprint-related rounding effects are visible. The influence of the laser footprint can be seen even more clearly in the point cloud of the power lines. Due to the large scan spot of the L1 sensor, the distribution of the laser beam energy over a relatively large area of more than 20 cm, object points are also detected, although the laser beam axis is already aiming past the power line. The smaller footprint of the high-end system (3 cm) enables precise reconstruction of linear objects. Finally, on a flat surface (road), Figure 7c shows the difference in quality, especially of the LiDAR unit. In the consumer-grade system, the points' dispersion amounts to 2 cm (1σ), while in the survey-grade system this is only 5 mm.

5. SUMMARY AND CONCLUSIONS

This paper discussed the technological differences between UAV laser scanners with geodetic precision requirements and consumer-grade instruments. The latter are mainly used in the automotive industry as for driver assistance systems but are also increasingly installed on UAVs for 3D mapping of topography and infrastructure. With the launch of the *DJI* Zenmuse L1, a complete measurement system consisting of GNSS, IMU, laser scanner and camera is now available at around 10K EUR, which is about an order of magnitude cheaper than high-end devices. An analysis based on the device specifications has shown that a point position accuracy of 5-10 cm can be expected for consumer-grade systems and that the spatial resolution of such inexpensive scanner systems is about 25 cm due to the large elliptical laser footprint despite a high point density of more than 50 points/m^2. The achievable spatial resolution is thus limited more by the quality of the laser beam than by the point density.

Based on measurements of a UAV LiDAR survey in Hessigheim (Baden-Württemberg, Germany) with a survey-grade sensor (*RIEGL* VUX-1UAV) in March 2021 and a consumer-grade system (*DJI* Zenmuse L1) in March 2022, the theoretical superiority of the high-end system was confirmed and also the limitations of the low-cost system in terms of trajectory accuracy, ranging accuracy, scan angle accuracy and laser beam quality were made transparent.

The International Archives of the Photogrammetry, Remote Sensing and Spatial Information Sciences, Volume XLVIII-1/W3-2023
2nd GEOBENCH Workshop on Evaluation and BENCHmarking of Sensors, Systems and GEOspatial Data
in Photogrammetry and Remote Sensing, 23–24 October 2023, Krakow, Poland

An attempt to re-calibrate the sensor system using rigorous strip adjustment revealed deficiencies of the scanning unit, which could not be compensated by the employed adjustment method. In future work, we plan to integrate more sophisticated calibration models for the Risley prism-based scanning unit of the Livox sensor (Brazeal et al., 2021) in the strip adjustment framework, which show a potential for further improvement of the georeferencing accuracy. Up to now, the relative orientation precision measured as height discrepancies in strip overlap areas is in the range of 4 cm. With improved scan angle calibration procedures, we expect a further improvement to 2-3 cm. The survey-grade sensors show precision and accuracy values in the area of 1 cm and, thus, will still outperform the consumer-grade sensors. This also applies to the 3D reconstruction capabilities, as the large laser footprint of the consumer-grade sensor entails blurring of small-scale details, which could be detectable if only the relatively high point density is considered.

Nevertheless, it can be stated that for moderate accuracy requirements in the dm-range, inexpensive, compact and lightweight laser scanning systems are now also available for surveying tasks that can be integrated on various UAV platforms such as multicopters and also fixed-wing aircraft.

REFERENCES

Alsadik, B., 2020. Multibeam Lidar for Mobile Mapping Systems. *GIM International*.

Altuntas, C., 2023. Review of Scanning and Pixel Array-Based LiDAR Point-Cloud Measurement Techniques to Capture 3D Shape or Motion. *Applied Sciences*, 13(11). https://www.mdpi.com/2076-3417/13/11/6488.

Brazeal, R. G., Wilkinson, B. E., Hochmair, H. H., 2021. A Rigorous Observation Model for the Risley Prism-Based Livox Mid-40 Lidar Sensor. *Sensors*, 21(14). https://www.mdpi.com/1424-8220/21/14/4722.

Colomina, I., Molina, P., 2014. Unmanned aerial systems for photogrammetry and remote sensing: A review. *ISPRS Journal of Photogrammetry and Remote Sensing*, 92, 79–97.

Cramer, M., Haala, N., Laupheimer, D., Mandlburger, G., Havel, P., 2018. Ultra-high precision UAV-based LiDAR and dense image matching. *International Archives of the Photogrammetry, Remote Sensing and Spatial Information Sciences*, 42.

Glira, P., Pfeifer, N., Mandlburger, G., 2016. Rigorous Strip Adjustment of UAV-based Laserscanning Data Including Time-Dependent Correction of Trajectory Errors. *Photogrammetric Engineering & Remote Sensing*, 82(12), 945–954.

Glira, P., Pfeifer, N., Mandlburger, G., 2019. Hybrid orientation of Airborne LiDAR point clouds and aerial images. 4(2/W5).

Haala, N., Kölle, M., Cramer, M., Laupheimer, D., Zimmermann, F., 2022. Hybrid georeferencing of images and LiDAR data for UAV-based point cloud collection at millimetre accuracy. *ISPRS Open Journal of Photogrammetry and Remote Sensing*, 4, 100014.

Jutzi, B., Stilla, U., 2006. Range determination with waveform recording laser systems using a Wiener Filter. *ISPRS Journal of Photogrammetry and Remote Sensing*, 61(2), 95–107.

Kersten, T., Wolf, J., Lindstaedt, M., 2022. Investigations into the accuracy of the UAV system DJI Matrice 300 RTK with the sensors Zenmuse P1 and L1 in the Hamburg test field. *The International Archives of the Photogrammetry, Remote Sensing and Spatial Information Sciences*, XLIII-B1-2022, 339–346.

Kölle, M., Laupheimer, D., Schmohl, S., Haala, N., Rottensteiner, F., Wegner, J. D., Ledoux, H., 2021. The Hessigheim 3D (H3D) benchmark on semantic segmentation of high-resolution 3D point clouds and textured meshes from UAV LiDAR and Multi-View-Stereo. *ISPRS Open Journal of Photogrammetry and Remote Sensing*, 1, 100001.

Liu, Z., Zhang, F., Hong, X., 2022. Low-Cost Retina-Like Robotic Lidars Based on Incommensurable Scanning. *IEEE/ASME Transactions on Mechatronics*, 27(1), 58–68.

Mallet, C., Bretar, F., 2009. Full-waveform topographic lidar: State-of-the-art. *ISPRS Journal of Photogrammetry and Remote Sensing*, 64(1), 1–16.

Mandlburger, G., 2022. Uav laser scanning. A. Eltner, D. Hoffmeister, A. Kaiser, P. Karrasch, L. Klingbeil, C. Stöcker, A. Rovere (eds), *UAVs for the Environmental Sciences - Methods and Applications*, wbg Academic, Darmstadt, 199–217.

Nex, F., Armenakis, C., Cramer, M., Cucci, D., Gerke, M., Honkavaara, E., Kukko, A., Persello, C., Skaloud, J., 2022. UAV in the advent of the twenties: Where we stand and what is next. *ISPRS Journal of Photogrammetry and Remote Sensing*, 184, 215-242.

Pfeifer, N., Mandlburger, G., Otepka, J., Karel, W., 2014. OPALS –- A framework for Airborne Laser Scanning data analysis. *Computers, Environment and Urban Systems*, 45, 125–136.

Pfennigbauer, M., Wolf, C., Weinkopf, J., Ullrich, A., 2014. Online waveform processing for demanding target situations. *Proc. SPIE*, 90800J.

Pöppl, F., Neuner, H., Mandlburger, G., Pfeifer, N., 2023. Integrated trajectory estimation for 3D kinematic mapping with GNSS, INS and imaging sensors: A framework and review. *ISPRS Journal of Photogrammetry and Remote Sensing*, 196, 287-305.

Schwarz, B., 2010. Mapping the world in 3D. *Nature Photonics*, 4(7), 429–430.

Schwarze, C. R., Schundler, E. C., Vaillancourt, R., Newbry, S. P., Benedict-Gill, R., 2013. Risley prism scan-based approach to standoff trace explosive detection. *Optical Engineering*, 53(2), 021110.

Shan, J., Toth, C. K. (eds), 2018. *Topographic Laser Ranging and Scanning: Principles and Processing*. 2nd edn, CRC Press, Boca Raton, FL.

Vosselman, G., Maas, H.-G. (eds), 2010. *Airborne and Terrestrial Laser Scanning*. Whittles Publishing, UK.

Wagner, W., Ullrich, A., Ducic, V., Melzer, T., Studnicka, N., 2006. Gaussian decomposition and calibration of a novel small-footprint full-waveform digitising airborne laser scanner. *ISPRS Journal of Photogrammetry and Remote Sensing*, 60(2), 100–112.